Article

Structure

Structural Insights into WD-Repeat 48 Activation of Ubiquitin-Specific Protease 46

Graphical Abstract

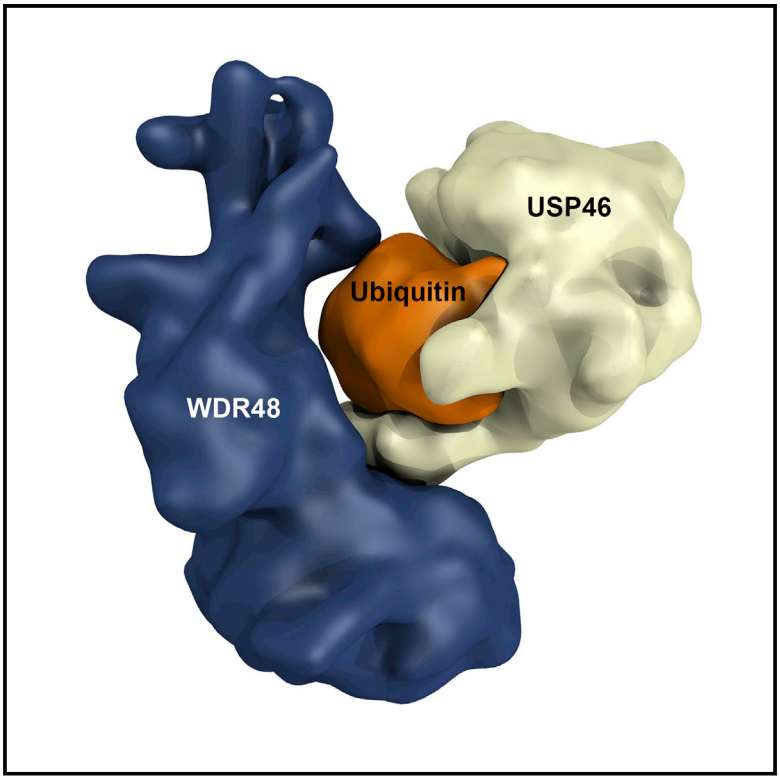

Authors

Jianping Yin, Allyn J. Schoeffler, Katherine Wickliffe, ..., Melissa A. Starovasnik, Erin C. Dueber, Seth F. Harris

Correspondence

harris.seth@gene.com (S.F.H.), dueber.erin@gene.com (E.C.D.)

In Brief

WD-repeat proteins have been identified as co-factors for USP family deubiquitinases. In a series of novel structures, Yin et al. describe an unprecedented interaction between WDR48 and USP46:ubiquitin. Binding and functional assays validate the interface and extend the insights to USP1, indicative of a prototypical example.

Highlights

- The WDR48:USP46:ubiquitin complex structure unveils unexpected interactions
- WDR48 stabilizes USP46 via contacts far removed from the deubiquitinase active site
- Select mutations validate the functional interface and extend the findings to USP1
- The WDR48 SUMO-like domain is poised to mediate substrate-complex interactions

Accession Numbers

5CVL
5CVM
5CVN
5CVO

Yin et al., 2015, Structure *23*, 2043–2054
November 3, 2015 ©2015 Elsevier Ltd All rights reserved
http://dx.doi.org/10.1016/j.str.2015.08.010

Structure
Article

Structural Insights into WD-Repeat 48 Activation of Ubiquitin-Specific Protease 46

Jianping Yin,[1] Allyn J. Schoeffler,[2] Katherine Wickliffe,[3] Kim Newton,[3] Melissa A. Starovasnik,[1] Erin C. Dueber,[2,*] and Seth F. Harris[1,*]
[1]Department of Structural Biology, Genentech, Inc., 1 DNA Way, South San Francisco, CA 94080, USA
[2]Department of Early Discovery Biochemistry, Genentech, Inc., 1 DNA Way, South San Francisco, CA 94080, USA
[3]Department of Physiological Chemistry, Genentech, Inc., 1 DNA Way, South San Francisco, CA 94080, USA
*Correspondence: harris.seth@gene.com (S.F.H.), dueber.erin@gene.com (E.C.D.)
http://dx.doi.org/10.1016/j.str.2015.08.010

SUMMARY

Protein ubiquitination patterns are an important component of cellular signaling. The WD-repeat protein WDR48 (USP1-associated factor UAF-1) stimulates activity of ubiquitin-specific proteases USP1, USP12, and USP46. To understand how WDR48 exerts its effect on the USP scaffold, we determined structures of the ternary WDR48:USP46:ubiquitin complex. WDR48 interacts with the USP46 fingers subdomain via a relatively small, highly polar surface on the top center of the WDR48 β propeller. In addition, WDR48 has a novel ancillary domain and a C-terminal SUMO-like domain encircling the USP46-bound ubiquitin. Mutation of residues involved in the WDR48:USP46 interaction abrogated both binding and deubiquitinase activity of the complex. An analogous mutation in USP1 similarly blocked WDR48-dependent activation. Our data suggest a possible mechanism of deubiquitinase stimulation via stabilization and prolonged residence time of substrate. The unprecedented mode of interaction between the USP fingers domain and the WD-repeat β propeller serves as a prototypical example for this family of deubiquitinases.

INTRODUCTION

Post-translational modification of proteins provides rich patterns of alterations with widespread functional consequences. Reversible covalent attachment of ubiquitin occurs via isopeptide linkage of the ubiquitin C terminus to substrate protein lysines. Polyubiquitin chains can extend from any of the seven lysine residues of ubiquitin itself, and diversity is further amplified by branching and the combinatorial possibilities of these varied linkages (Komander and Rape, 2012). These modifications are important in targeting proteins to the proteasome (Hershko et al., 1982), as well as in an expansive set of non-degradative roles: regulating DNA repair (Nijman et al., 2005), signaling, transcription (Köhler et al., 2010; Samara et al., 2010), cell-cycle control (Teixeira and Reed, 2013), mitochondrial integrity (Bingol et al., 2014), and the generation and recycling of free ubiquitin (Reyes-Turcu and Wilkinson, 2009).

A large set of ~95 known deubiquitinases (DUBs) comprising five families regulates specific removal of ubiquitin. Among these, the ubiquitin-specific proteases (USPs) form the largest group, with 58 members that share a common catalytic domain of ~350 amino acids (Komander et al., 2009). Insertions variously elaborate the core USP scaffold such that the largest members exceed 1,000 residues in length (Komander et al., 2009; Ye et al., 2009). The conserved USP architecture features "thumb" and "palm" subdomains that bear the Cys-protease catalytic triad (Cys, His, Asp), while an extended "fingers" subdomain, often including a zinc-coordinating motif, helps cradle ubiquitin and orient its C terminus toward the catalytic active site.

Several free USP structures (e.g. USP14, USP8) show features incompatible with enzymatic activity, whether due to ubiquitin-proximal loops (Hu et al., 2005), non-productive catalytic residue and "switch loop" orientation in USP7 (Faesen et al., 2011a), or inward motion of the fingers domain (Avvakumov et al., 2006). Binding of ubiquitin substrate imparts conformational changes in these examples, notably motions of the fingers domain as well as USP loops near the ubiquitin site and the catalytic center, into ubiquitin-accommodating conformations (Hu et al., 2002; Molland et al., 2014).

Two studies of allosteric USP binding partners have shown direct contacts with features in close proximity to the USP active site and the palm and thumb domains. The C-terminal ubiquitin-like domains (UBL) 4 and 5 of USP7 appear to mediate stimulatory effects through intramolecular contact with the USP7 switching loop, an interaction further potentiated through stabilization of USP7 UBL1-3 by guanosine monophosphate synthetase (Faesen et al., 2011a). Structures of the yeast SAGA DUB module describe intertwined co-factors (Sus1, Sgf75, and Sgf11) that form an intricate set of scaffolding interactions packing against the palm and thumb subdomains of the USP fold Ubp8. These co-factors thereby organize the active site and provide a measure of global Ubp8 stabilization to balance its intrinsic flexibility (Köhler et al., 2010; Samara et al., 2010).

Detailed understanding of the mechanism of DUB activation by partner proteins has remained challenging. In a proteomic screen, numerous WD-40 repeat proteins, named for a signature Trp-Asp repeat and typically found as β-propeller scaffolds in diverse protein complexes, were implicated in interactions with 20 different USPs (Sowa et al., 2009). WDR48 (also known as USP1-associated factor 1, UAF-1) stimulates the activity of

USP1 (Cohn et al., 2007) as well as that of two smaller homologs, USP12 and USP46 (Cohn et al., 2009). USP1 regulates DNA-damage response, specifically the Fanconi anemia and translesion DNA synthesis (TLS) pathways, by deubiquitination of FANCD2 and PCNA substrates to affect their recruitment of DNA repair complexes to damage sites (Huang et al., 2006; Murai et al., 2011; Park et al., 2013; Yang et al., 2011). Heightened USP1 activity maintains cells in an undifferentiated state in the context of osteosarcoma, as deubiquitination of ID (''inhibitors of DNA binding'') transcription factors leads to their increased stability and antagonism of differentiation-promoting basic helix-loop-helix transcription factors (Williams et al., 2011). Prominent in DNA repair, USP1 is a potential target for cancer therapy (Chen et al., 2011; García-Santisteban et al., 2013; Liang et al., 2014; Villamil et al., 2013). USP12 is a component of the Akt signaling pathway (Gangula and Maddika, 2013), with ties to androgen receptor activation (McClurg et al., 2014). Both USP12 and USP46 deubiquitinate histone H2A and H2B, affecting *Xenopus* development (Joo et al., 2011), and, unlike USP1, these smaller USPs can simultaneously bind WDR20 in addition to WDR48 (Joo et al., 2011; Kee et al., 2010). USP1, 12, and 46 may also be involved in papillomavirus propagation, as the viral E1 protein recruits these DUBs to its origin of replication via interaction with WDR48, and abrogation of their deubiquitinase activity significantly reduces viral replication (Lehoux et al., 2014).

USP1, 12, and 46 are unified by their dependence on WDR48, which stimulates their activities by approximately 10- to 30-fold. This effect may be mediated more by altering turnover (k_{cat}) rather than substrate affinity or K_M (Cohn et al., 2007; Faesen et al., 2011b). Binding of USP1 by WDR48 was sensitive to deletions within the WD-repeats, indicating the importance of a presumed propeller domain (Cohn et al., 2007). Efforts to map complementary WDR48-interacting regions of USP1 proposed either a portion of the fingers domain (420–520) (García-Santisteban et al., 2012) or a non-conserved insertion (235–408) that includes Ser313 whose phosphorylation was reported to affect the interaction (Villamil et al., 2012b). This latter possibility is surprising given that USP12 and 46 also bind WDR48, but lack this insertion. Recent studies corroborate that Ser313 is not critical for USP1:WDR48 binding and function (Olazabal-Herrero et al., 2015).

To elucidate these aspects of WDR48:USP interaction and biology, we report the crystal structures of ternary complexes of WDR48:USP46∼ubiquitin, a binary complex of USP46∼ubiquitin, and free WDR48. Structure-based mutagenesis combined with direct binding and functional assays validate our observed WDR48:USP46 interface. Moreover, mutagenesis of equivalent residues in the WDR48:USP1 system abrogates both USP1 binding to WDR48 and deubiquitination of a USP1 substrate in cells, suggesting that this interface, distinct from prior USP interactions described, may serve as a prototypical example of activity-modulating β-propeller:USP family interactions.

RESULTS

WDR48 Contains a β-Propeller and a Novel-Fold Ancillary Domain

To aid crystallization, we identified a stable C-terminal deletion of WDR48 that excludes the last 97 amino acids (Figure S1). The structure of $WDR48_{2–580}$ reveals a β-propeller domain (residues 27–360) and a curved ancillary domain (13–24 and 362–561) of novel fold (Table 1; Figure 1). The relatively canonical seven-bladed β propeller creates a toroid with a narrow central pore. Modest insertions are present within blades 3 (12-residue insertion 146–168) and 7 (26-residue insertion 327–353, of which 337–345 are disordered in our structure) on the outer bottom surface of the toroid. Many propellers have a circularly closed topology as a first amino-terminal strand contributes to the final blade (Figure S2). Here, the seventh blade has a full complement of four strands while the WDR48 amino-terminal residues 13–24 are unexpectedly incorporated as an integral strand within the ancillary domain rather than the propeller (Figure 1). This results in proximal positioning of the interdomain tethers that leaves the top of the propeller relatively exposed, and may enable hinged motions between the propeller and ancillary domains.

The ancillary domain is offset to one side of the propeller ring, centered over blades 1 and 2. A 3D similarity search (Dali [Holm and Sander, 1995]) indicates a novel overall fold while also identifying a propeller blade as a substructure embedded within the ancillary domain architecture. This curved blade, formed from an additional eighth WD-repeat in the WDR48 primary sequence, is stacked on a second arched, five-stranded β sheet that includes the N-terminal strand (Figure 1). The outer convex faces of those curved sheets pack against loops and short α helices out to the last discernible residue (561), which terminates on the upper face of the ancillary domain, away from the β propeller.

Binary Complex of USP46∼Ubiquitin

We determined the 1.9-Å resolution structure of a covalently coupled $USP46_{25–366}$∼ubiquitin complex (Table 1). The structure shows a canonical USP architecture with thumb, palm, and extended fingers subdomains (Figure 2). Ubiquitin substrate is cradled between the fingers and the inner palm/thumb regions with its C-terminal sequence leading into the cysteine protease active site, where the conjugated ubiquitin G76 is covalently linked to the catalytic USP46 C44. The tip of the fingers domain features a zinc ribbon motif with a coordinated zinc ion. The USP46:ubiquitin interface buries ∼1,825 $Å^2$ of surface area on each protein. Ubiquitin-proximal loops, the ''switching'' loop equivalent, and the catalytic center all have unambiguous electron density showing their contacts with ubiquitin and its C-terminal tail. Similar to many USP homologs, USP46 has an insertion at the junction of the thumb and fingers domains that is disordered in our model (USP46 residues 143–163); USP1 has here a larger 195-residue insertion. The preceding helix (αE) provides a central shaft to the USP46 architecture, and it continues several turns beyond the main body of the protein as it leads into this disordered gap. Annotated comparisons between USP structures are shown in Figure S3.

WDR48 Contacts USP46 via a β-Propeller:USP46 Fingers Interaction

To analyze the interactions of these proteins in a ternary complex, we crystallized and determined the 3.35-Å resolution structure of $WDR48_{2–580}$ bound to a $USP46_{25–366}$∼ubiquitin conjugate (Table 1). The WDR48 β-propeller domain (residues 27–360) provides a platform for interaction at the toroid's top center to bind the very distal portion of the USP46 fingers domain on the outer

Table 1. Data Collection and Refinement Statistics

	$WDR48_{2–580}$	USP46∼Ubiquitin	$WDR48_{2–580}$:USP46∼Ubiquitin	WDR48:USP46∼Ubiquitin
Data Collection				
Space group	$I4_122$	$C222_1$	I222	C2
Cell dimensions				
a, *b*, *c* (Å)	139.5, 139.5, 235.1	90.6, 105.1, 134.7	103.4, 154.2, 182.9	211.3, 103.8, 191.0
α, β, γ (°)	90, 90, 90	90, 90, 90	90, 90, 90	90, 119.0, 90
Resolution (Å)	50–3.0 (3.11–3.0)	50–1.9 (1.967-1.9)	50–3.35 (3.49–3.35)	50–3.88 (4.02–3.88)
R_{merge}	0.13 (0.85)	0.067 (0.77)	0.12 (0.72)	0.17 (0.69)
$I/\sigma I$	19.4 (3.2)	16.3 (2.4)	13.8 (2.8)	5.7 (1.4)
Completeness (%)	99.9 (99.1)	98.9 (97.8)	99.6 (96.1)	93.6 (82.3)
Redundancy	16.1 (16.5)	6.2 (6.0)	7.7 (7.7)	3.5 (3.1)
Wilson *B* factor	66.9	29.4	88.8	79.2
Phasing FOM	0.259	–	–	–
Phasing Sites	8 Au	–	–	–
Refinement				
Resolution (Å)	50–3.0 (3.11–3.0)	50–1.9 (1.967–1.9)	50–3.35 (3.49–3.35)	50–3.88 (4.02–3.88)
No. of reflections	380,955 (37,958)	311,236 (29,475)	162,990 (15,378)	110,113 (8,555)
R_{work}/R_{free}	0.1892/0.2336	0.1887/0.2243	0.1952/0.2701	0.2235/0.2719
No. of atoms	4,316	3,675	7,350	15,556
Protein	4,139	3,185	7,315	15,554
Ligand/ion	17	1	1	2
Water	160	489	34	0
Average *B* factors	71.0	32.5	57.5	58.7
Protein	71.1	30.6	57.7	58.7
Ligand/ion	125.8	23.3	86.9	86.9
Water	61.1	44.7	30.0	NA
Root-mean-square deviations				
Bond lengths (Å)	0.014	0.004	0.014	0.012
Bond angles (°)	1.98	0.84	1.96	1.54
Ramachandran (%)				
Favored	91.0	97	92	93[a]
Outliers	0.77	0.52	1.2	0.81[a]
Clashscore	5.43	3.46	13.96	11.14

[a]The full-length WDR48:USP46∼ubiquitin complex includes only a poly-ala trace of the C-terminal residues (563–671) and was refined using Ramachandran restraints.

surface of the zinc-coordinating motif (Figure 3). The relatively small (720 $Å^2$ buried surface area) but well-packed junction includes many charged and polar side chains extending from each partner (Figure 3B). The USP fingers lie between ubiquitin and the WDR48 β propeller with the coordinated zinc ion of USP46 poised above the central pore of the propeller. Unexpectedly, this "interface-1" leaves the bulk of USP46 quite removed from WDR48, as the active-site Cys44 is ∼41 Å from the nearest WDR48 residue. The USP46-bound ubiquitin is closer, however, sheltered adjacent to the concave inner face of the WDR48 ancillary domain. Surprisingly, there is a small gap and no direct contacts between WDR48 and ubiquitin, despite a seeming shape complementarity of the nearby surfaces (Figures 3C and 3D).

Alignment of our separate structures onto the complex shows very little conformational change (Figure S4) (Cα root-mean-square deviation for isolated versus complex-bound species: WDR48 = 1.4 Å, USP46∼ubiquitin = 1.1 Å, ubiquitin only = 0.3 Å.) For WDR48, the only large shift occurs in the extended loop of blade 3 (residues 149–160, Figure S4) where a symmetry-related USP46 neighbor packs between this outside region of the β propeller and the adjoining ancillary domain helix E (residues 537–545). This second interface ("interface-2") is mediated by two β strands of USP46 (residues 281–295) that form hydrogen bonds extending the β sheet of WDR48 blade 2 (Figure 4). This interface occludes slightly more surface area (1,112 $Å^2$) than observed for interface-1, but is somewhat less compelling in its prevalence of sequence-insensitive backbone interactions, the outward orientation of ubiquitin relative to the WDR48, and that it again leaves the USP46 active site relatively distant (Cys44 is ∼31 Å from the nearest WDR48 residue). While protein interactions are most common on the top of β-propeller scaffolds, examples also exist using side, loop, and bottom surfaces (Xu and Min, 2011). We therefore designed

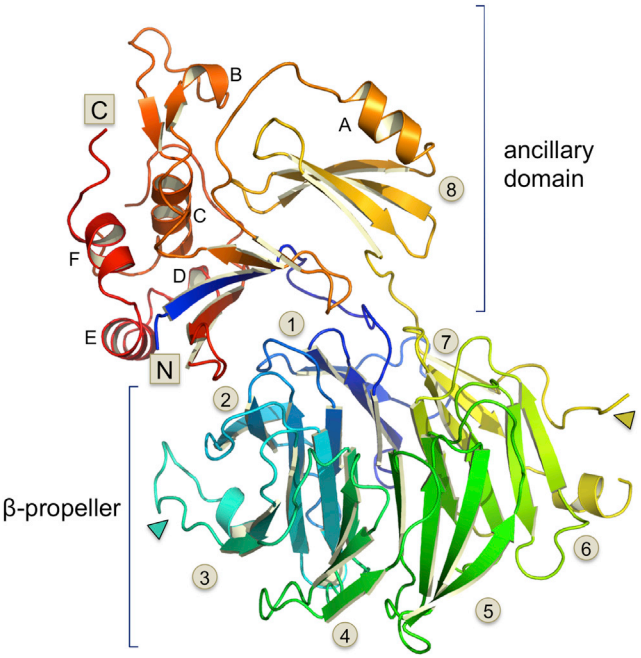

Figure 1. Structure of WDR48

WDR48 is colored blue (N terminus) to red (C terminus). The view is oriented looking obliquely onto the β-propeller top surface (blades numbered 1–7), followed by the ancillary domain including an eighth propeller blade substructure (marked 8). Helical features in the ancillary domain are labeled alphabetically from A to F. Electron density was not interpretable beyond residue 561, marking the C terminus of the ancillary domain at the upper left of the figure. See also Figure S2.

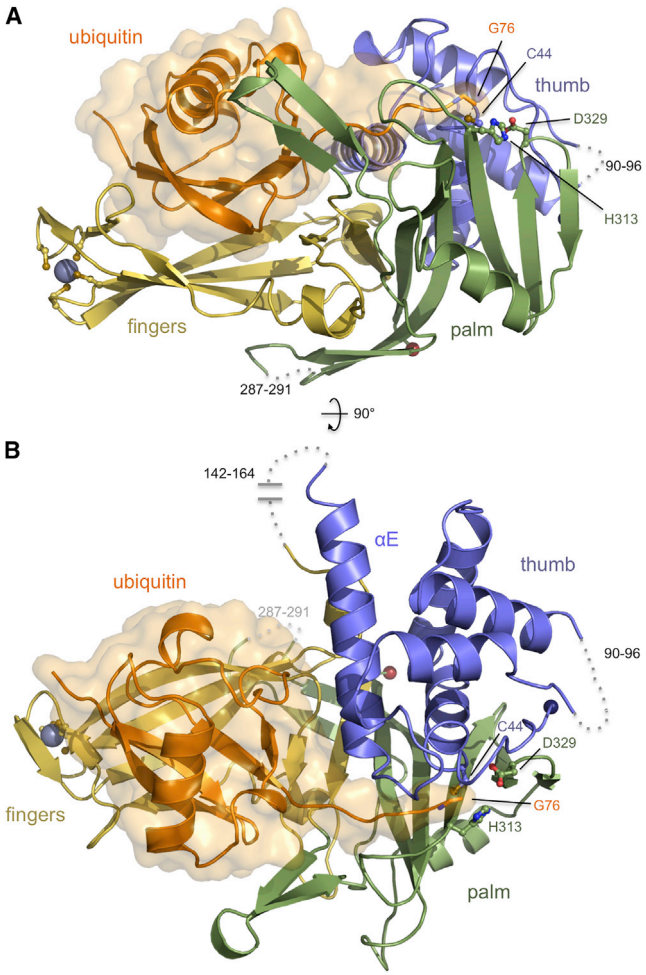

Figure 2. USP46$_{25–366}$~Ubiquitin Structure

USP46$_{25–366}$~ubiquitin structure is colored as USP46 thumb (blue), palm (green), and fingers (gold) domains with bound ubiquitin (orange). The zinc ribbon cysteines are shown as sticks at the tip of the fingers domain coordinating a zinc ion (gray sphere). Ubiquitin G76 is covalently attached to the USP46 active site C44 (with catalytic residues H313 and D329 also shown as sticks). Disordered loops are indicated with dashed lines and residue number boundaries.

(A) Side view showing the extended fingers domain cradling ubiquitin and the passage of the C-terminal ubiquitin segment.

(B) Top view highlights the long central helix of the USP thumb domain (αE) that leads to the disordered linker (142–164) between conserved thumb and fingers elements at the top of the image.

See also Figure S3.

structure-based mutations to provide rigorous experimental proof as to which interface is functionally relevant for USP activation.

In interface-1 we created a WDR48 triple mutation of K214E/W256A/R272D (termed WDR48$_{3X}$) to alter the charge property and surface shape of WDR48. We additionally mutated WDR48 S170Y, which we anticipated would cause a steric clash with USP46 in the observed interface-1 interaction (Figure 3B). USP46 E186 makes several contacts to the K214/W256/R272 patch of WDR48, so we also created a USP46 E186K charge reversal to test for disrupted binding and function. Interface-2's β-sheet interactions with WDR48 had much less reliance on side chains and thus offered fewer opportunities for obvious disruptive mutations. We selected L152R/S155W on the WDR48 blade 3 insertion, as these outward-oriented larger amino acid substitutions are expected to create a steric clash with the observed position of USP46 (Figure 4B).

USP46 In Vitro Assays Confirm the Importance of Interface-1

USP46 and WDR48 variants were tested for interaction via a direct binding assay. WDR48 L152R/S155W mutations in interface-2 had minimal impact on WDR48:USP46 association (Figure 5A). By contrast, WDR48 mutation S170Y of interface-1 greatly reduced the observed interaction. An even more striking effect was observed for WDR48$_{3X}$, which had no detectable interaction with (WT) USP46, thus confirming the importance of interface-1 for binding between these two proteins. In addition, WDR48$_{3X}$ interaction with USP46 was partially restored by the USP46 E186K charge-reversal mutant. Together these complementary mutants showed weak but measurable binding (K_d = 3.6 μM, Figure S5). WT WDR48:USP46 has a surprisingly tight affinity (0.1 nM with a slow k_{off}) given the small size of the interface observed in the structure; however, unlike many protein-protein interfaces, the USP46-WDR48 interface is mainly composed of charged interactions, not buried hydrophobic residues. Our kinetic analysis also revealed that the reduced binding of the S170Y mutant (~100 nM) is primarily a result of

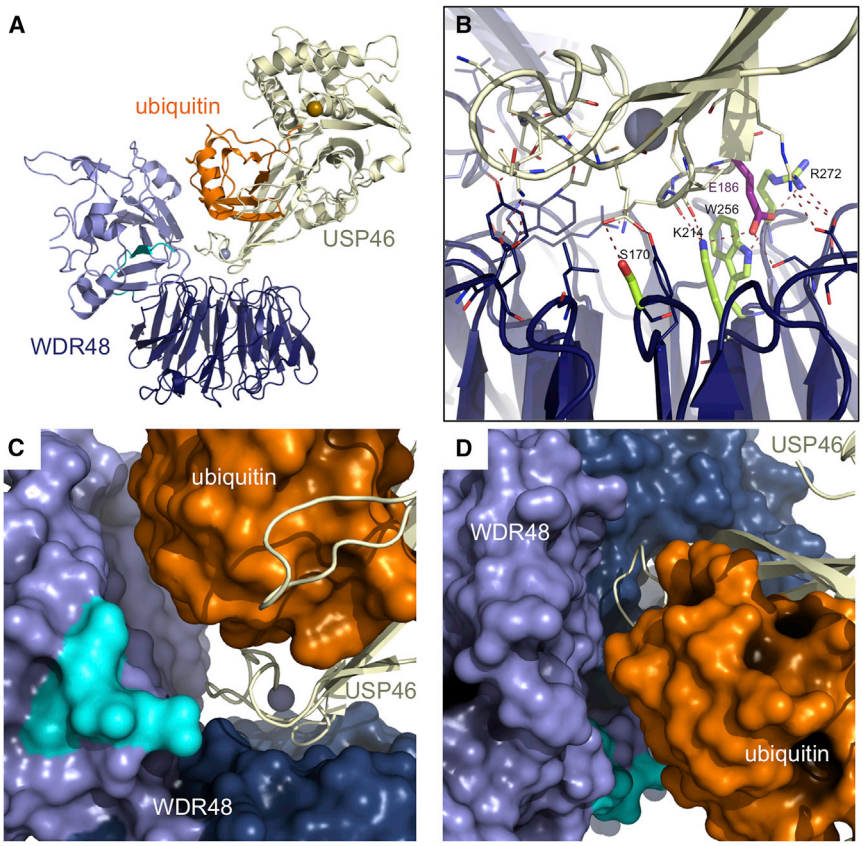

Figure 3. WDR48$_{2–580}$:USP46$_{25–366}$~Ubiquitin Complex

WDR48 propeller (dark blue), ancillary domain (light blue, N-terminal strand in cyan), USP46 (ivory), and ubiquitin (orange) are colored. Spheres mark the coordinated zinc ion (gray) at the outer USP46 fingertips and the sulfur atom of the DUB catalytic site cysteine (gold).

(A) WDR48:USP46 interface-1 with the USP46 fingertips directly over the top center of the β propeller. The active-site Cys sulfur atom is ~41 Å from the nearest WDR48 residue.

(B) Closer view of interface showing amino acid side chains involved in the WDR48:USP46 interaction. Residues selected for mutagenesis are labeled and emphasized in green (WDR48) or magenta (USP46).

(C and D) Molecular surfaces of WDR48 (β propeller, navy; ancillary domain, slate blue; N-terminal strand, cyan) and ubiquitin (orange) juxtapose a ribbon representation of USP46 (ivory) in the ternary complex interface-1 arrangement. (C) Oriented as (A), the USP46 fingers lie between WDR48 and ubiquitin. The zinc ion (gray sphere) is positioned over the β-propeller pore. The WDR48 ancillary domain has a gently curved inner wall that complements ubiquitin's surface, but a small gap remains between the two proteins. (D) View is rolled ~90° toward the viewer.

See also Figure S4.

a faster k_{off} relative to WT protein, while maintaining similar k_{on} (see Figure 5C).

The functional impact of the mutations was gauged in vitro using a ubiquitin-AMC (7-amino-4-ethylcoumarin) substrate in which cleavage by USP46 liberates the fluorescent dye. Consistent with the binding assay, WDR48 L152R/S155W showed stimulation of the USP46 reaction rate similar to that of WT WDR48 (Figure 6). In contrast, at 200-nM concentrations of USP46 and WDR48, both of the interface-1 mutation combinations tested abrogated WDR48 stimulation such that reaction rates were indiscernible from our negative control of USP46 alone. At a higher WDR48 concentration (4 μM, 20-fold molar excess over USP46), the S170Y mutant showed a weak stimulation of USP46 activity, while the WDR48$_{3X}$ mutant stimulation remained undetectable, a pattern that correlates exactly with the binding measurements. In this in vitro setting, a construct consisting of only the WDR48 β propeller (27–359) was able to stimulate USP46 almost as well as the full-length WT WDR48 construct, again corroborating the importance of interface-1, which, unlike interface-2, is contained wholly within the β-propeller domain. Finally, similar to the weak rescue of WDR48$_{3X}$ binding, USP46 E186K showed slightly better activity in the presence of WDR48$_{3X}$ compared with negligible stimulation by WT WDR48 (Figure S6C). All WDR48 reagents were tested alone in this assay to ensure a lack of any contaminating deubiquitinase activity (Figure S6A). Mutation of the catalytic cysteine 44 to serine in USP46 also demonstrated that the unstimulated rates observed for our designed mutants were in the regime of the catalytically dead deubiquitinase, and that stimulation was dependent on USP46 catalytic activity (Figure S6B).

USP1 Cellular Assays

To test whether the functional significance extends to more distantly related deubiquitinases, we examined binding and deubiquitination in USP1-based cellular assays. USP1 has but 17% identity with USP46 and includes several larger insertions. In light of the binding mode indicated by our structures, we designed the USP1 E444K mutation, homologous to USP46 E186K. We also created USP1 mutation S313A that was previously implicated as a phosphosensitive WDR48-interaction point (Villamil et al., 2012b).

WT and mutant WDR48 and USP1 constructs were transfected in 293T cells and tested in co-immunoprecipitation assays. As seen in Figure 7A, WDR48 co-immunoprecipitates efficiently upon pull-down of FLAG-tagged WT USP1, but has no visible interaction with the E444K USP1 mutant, corroborating our in vitro observations with USP46 E186K. In contrast, in our assay USP1 S313A is as robust as WT USP1 for co-immunoprecipitation of WDR48. Mutant WDR48 was also tested in an HA-tagged format. WT WDR48 (HA tag) efficiently precipitated with FLAG-tagged USP1 while interaction with the WDR48$_{3X}$ mutant could not be detected (Figure 7B).

USP1 E444K was further assayed for its ability to deubiquitinate the transcription factor ID2. Monoubiquitinated ID2 was identified as a biological substrate of USP1 in the context of cellular differentiation in osteosarcoma (Williams et al., 2011).

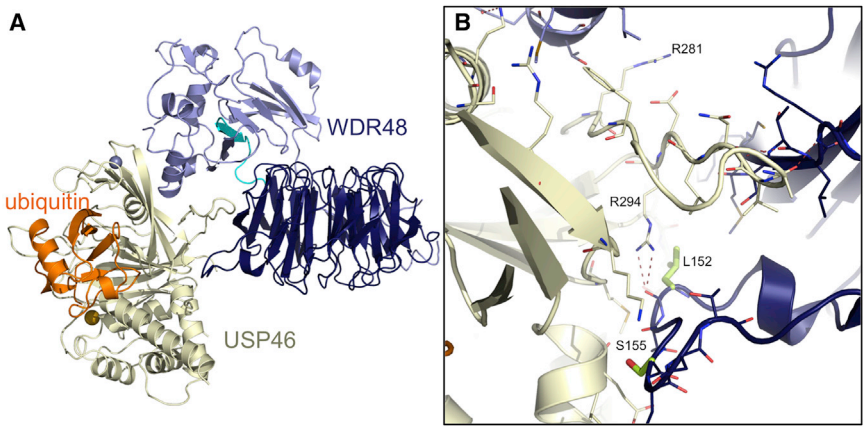

Figure 4. Interface 2 between WDR48 and USP46 Represented as in Figures 3A and 3B

(A) An extended loop of USP46 is bound between the side of the WDR48 β propeller and its ancillary domain.

(B) Close-up showing contributions from the WDR48 ancillary domain helix at the top of the figure, the blade 2 β sheet at right, and the blade 3 insertion below that surround the USP46 loop (residues 281–294). WDR48 residues selected for mutation (L152, S155) are emphasized as green sticks.

USP1 and WDR48 were transfected with ID2 (FLAG tag) and ubiquitin (HA tag). Sample loads were normalized for total ID2 (Figure 7C, α-FLAG WB box) allowing appreciation of the varying levels of ubiquitinated ID2 upon USP1 modulation. In the absence of transfected USP1, ID2 is present in a ubiquitinated form (Figure 7C, lane 2) that leads ultimately to its degradation (see absence of α-FLAG ID2 signal in "input" section in this lane). Transfection of WT USP1 leads to the expected dramatic reduction of Ub-ID2 by deubiquitination (lane 3). Upon transfection of catalytically inactive USP1 (C90S, lane 5), ubiquitinated ID2 levels are maintained, similar to the control lacking USP1 transfection (lane 2). The USP1 E444K mutation (lane 4) has an intermediate effect, as it does show some reduction of Ub-ID2, though not to the extent observed for WT protein. Given that transfected proteins including USP1 E444K are highly overexpressed, we interpret even this moderate persistence of the monoubiquitinated ID2 as a significant abrogation of deubiquitinase function in the E444K setting. Taken together, our series of experiments points to this being a result of diminished interaction with the stimulatory WDR48 co-factor, and provides evidence that USP1 shares a similar mode of interaction with WDR48 as observed in our structure of the WDR48:USP46∼ubiquitin ternary complex.

The Full-Length WDR48 Ternary Complex Suggests a Ubiquitin-Proximal WDR48 C-Terminal SUMO-like Domain

We crystallized a ternary complex that included full-length WDR48 bound to the $USP46_{25–366}$∼ubiquitin conjugate. While the ∼4-Å diffraction limit of these crystals was not sufficient for de novo construction of the missing putative SUMO-like domain (SLD) of WDR48 (Yang et al., 2011), a clear solvent-protein boundary and strong statistics validated the $WDR48_{2–580}$:$USP46_{25–366}$∼ubiquitin complex molecular replacement solution we identified. Furthermore, difference density indicating the missing domain clearly extended from our extant WDR48 C terminus, encircling the USP46-bound ubiquitin and approaching the thumb subdomain of USP46 over the top of the ubiquitin molecule (Figures 8 and S7). We identified 3 α-helical features within this density that guided positioning of a high-resolution SUMO model (PDB: 2LAS) whose topology traced all the significant observable features in the lower-resolution maps. Furthermore, while end points were not considered while positioning SUMO, the final pose showed compelling alignment of the SUMO amino terminus within density directly adjacent to its prescribed attachment point on our WDR48 structure (Figure S7F). While the limited side-chain detail precludes any sequence registration, these results indicate that the C-terminal domain of WDR48 adopts a modified SUMO-like fold with slightly longer helical insertions. Built here as a polyalanine trace, the fully elaborated SLD domain would contact ubiquitin, and is in a compelling orientation relative to the USP46∼ubiquitin conjugate (Figure 8).

DISCUSSION

WD-repeat proteins, one of the most populous families in eukaryotes, are heavily involved in interactions with USP members of the DUB family (Cohn et al., 2007; Sowa et al., 2009). We have elucidated a detailed view of WDR48 in complex with USP46∼ubiquitin. A charged surface atop the WDR48 β-propeller platform creates the primary binding interface contacting the zinc ribbon module on the outer and very distal tip of the USP46 fingers domain. Notably removed from the USP46 active site, the interface is completely distinct from prior examples in activation of either USP7 by its UBL domains (Faesen et al., 2011a) or stabilization of the yeast Ubp8 in the deubiquitinase module of the SAGA complex (Köhler et al., 2010; Samara et al., 2010). In those cases, the involvement of active-site proximal palm/thumb surfaces makes it simpler to envision how stimulatory co-factors could influence specific active-site arrangement and thereby affect enzymatic turnover (k_{cat}) more than substrate binding per se (K_M). Such a k_{cat}-oriented activation mechanism has also been ascribed to WDR48's effects on USP proteins (Cohn et al., 2007; Faesen et al., 2011b; Villamil et al., 2012a). Given the distinct binding mode elucidated here, it is less straightforward to reconcile this structure with direct active-site modulation, yet we propose a mechanism centered on WDR48-dependent USP stabilization that is consistent with implications from our observations and k_{cat} modulation.

The WDR48 propeller alone is sufficient to activate USP46 almost as well as full-length WDR48 (Figure 6). The high-resolution USP46∼ubiquitin structure derives from crystals that grew in the presence of the $WDR48_{2–336}$ propeller domain. Similarly, despite the chemically reactive warhead on modified ubiquitin, successful generation of the USP46∼ubiquitin adduct required WDR48 (see Experimental Procedures). While inconclusive of the absolute state of USP46 in solution, we were able to obtain

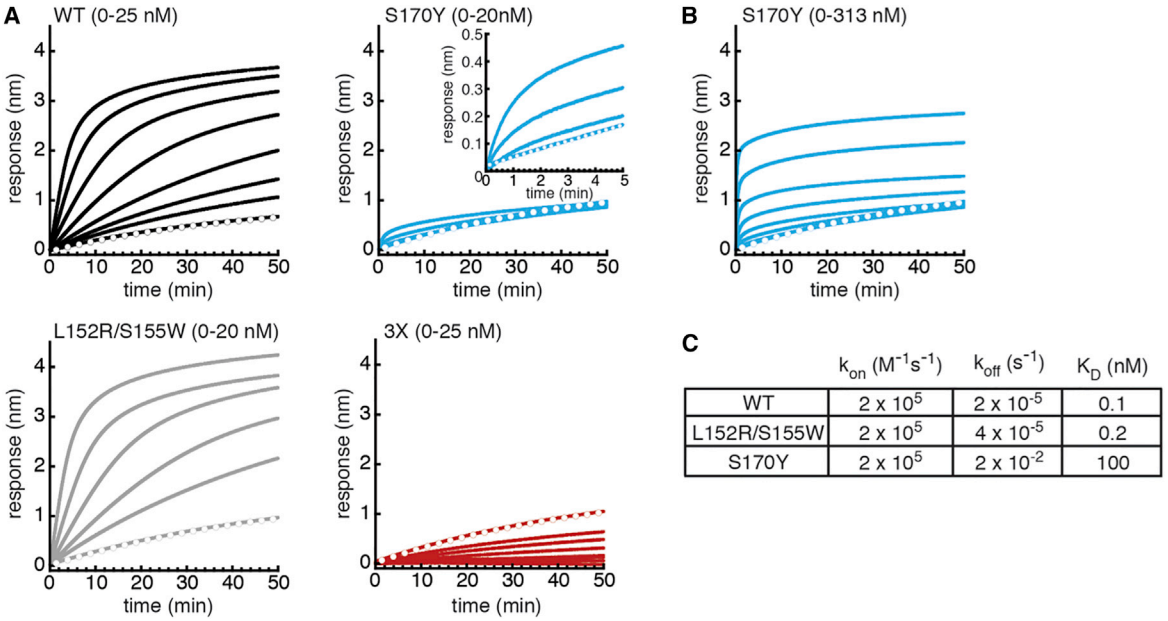

Figure 5. Direct Binding of WDR48 Variants to Singly Biotinylated USP46 as Measured by Biolayer Interferometry

(A) Raw sensorgrams show the association of WDR48 variants to immobilized USP46 (plotted as nm response as a function of time) for a similar range of analyte concentrations (WT and $WDR48_{3X}$, 0–25 nM; L152R/S155W and S170Y, 0–20 nM). Zero-analyte sensorgrams are denoted by open circles. Inset shows zoom of S170Y sensorgrams.

(B) Raw sensorgrams for a broader range of S170Y analyte concentration (0–313 nM) confirms binding above background.

(C) Zero-analyte controls were subtracted from sensorgrams in (A) and (B) and the resulting data fit to determine k_{on}, k_{off}, and K_D for each variant (see Experimental Procedures and Figure S5).

crystals of apo USP46, but poor diffraction led only to a partial molecular replacement solution in which the bulk of the fingers domain was not apparent in the electron density (data not shown). Taken together, these observations suggest a mode of activation whereby WDR48 stabilizes the otherwise labile USP46 through direct interaction with the distal region of the USP46 fingers with possible indirect allosteric effects on the active-site configuration. In isolation, USP1, USP12, and USP46 are relatively inefficient enzymes with slow turnover (Faesen et al., 2011b), which may be tied to transient, non-productive interactions between enzyme and substrate. Stabilization of a malleable apo USP46 to favor an active conformation would shift the equilibrium of association and promote productive interaction between ubiquitin and USP46. While we anticipate a similar

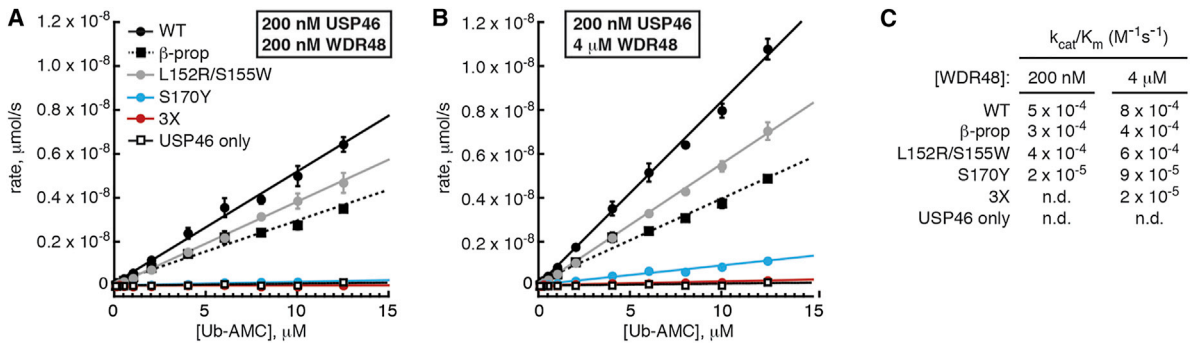

Figure 6. Activation of USP46 Catalytic Activity by WDR48 Variants

(A) Addition of 200 nM WT (black circles), β-propeller domain (black squares), or L152R/S155W (gray circles) WDR48 variant activates 200 nM USP46 to cleave a Ub-AMC substrate, whereas WDR48 mutations within interface 1 (S170Y, blue circles; $WDR48_{3X}$, red circles) show minimal activity comparable with the USP46 alone control.

(B) Similar results were obtained at 20-fold molar excess of WDR48 variants over USP46 (4 μM). For (A) and (B) the average rate of Ub-AMC cleavage (μmol/s) is plotted as a function of Ub-AMC concentration, where error bars represent standard deviations (n = 3).

(C) While the data in (A) and (B) do not support explicit determination of k_{cat} and K_M values, the ratio of k_{cat}/K_M was determined from the slopes of the linear fits of the data.

See also Figure S6.

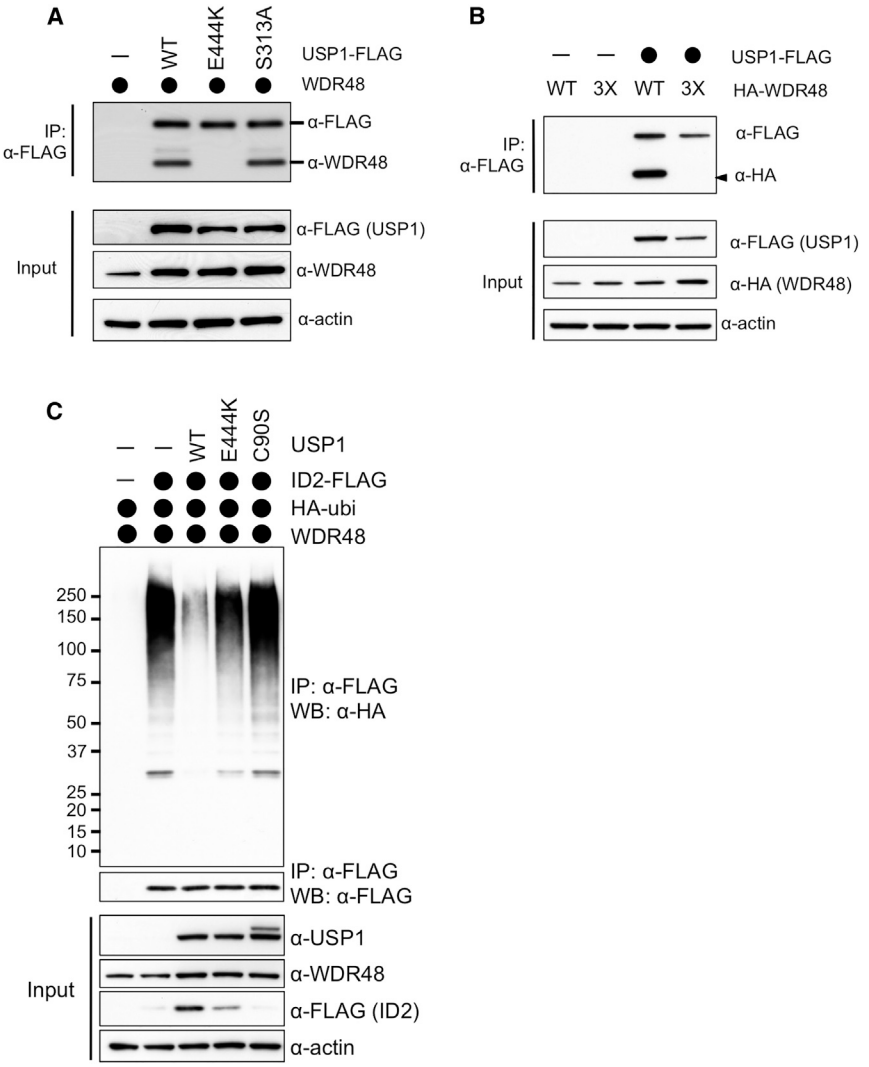

Figure 7. Co-immunoprecipitation of USP1 and WDR48 and Cellular Deubiquitination of ID2 by USP1

(A) WDR48 co-immunoprecipitates with both WT and S313A FLAG-tagged USP1, while the E444K USP1 mutant abrogates such interaction.

(B) WT WDR48 co-immunoprecipitates with FLAG-tagged USP1 (lane 3), while the WDR48 triple mutant (3X) does not (lane 4).

(C) Transfection of ID2-FLAG, HA-ubiquitin, and WDR48 leads to observation of a mono-ubiquitinated ID2 band (lane 2, upper panel), which is targeted for degradation (minimal intensity of α-FLAG "input"). Lanes were normalized for total ID2 (see α-FLAG WB in first subpanel). Inclusion of transfected WT USP1 results in ID2 deubiquitination (lane 3). Transfection of USP1 E444K shows diminished deubiquitination (lane 4), though not to the extent of the catalytically impaired USP1 C90S (lane 5).

mode of interaction for some WD-repeat proteins, the USP12 and USP46 co-factor WDR20 has low sequence homology to WDR48, and purification of a WDR20:WDR48:USP ternary complex (Kee et al., 2010) indicates that distinct propeller:USP interaction modes are likely to be found as well.

Beyond the propeller domain, we suggest that the C-terminal region of WDR48 is poised for roles in coordination of cellular co-factors and ubiquitin. The architecture of full-length WDR48 further elaborates this notion. The post-propeller WDR48 ancillary domain displays a concave ubiquitin-encompassing arch whose interior surface is more reminiscent of a chaperone-like environment designed to sterically shield the ubiquitin without specific interaction. Our experimental density for the intact WDR48 ternary complex, however, does indicate a small region of contact between the WDR48 C-terminal SLD domain and ubiquitin. It will be important to explore the nature of this contribution, whether as a ubiquitin-sensing domain, a surrogate cap replacing a cleaved polyubiquitin extension, or a simple C-clamp shape providing further stabilization compared with the "open-faced" binding of the propeller alone, or, more speculatively, whether this small WDR48 contact may abet turnover in clearing spent ubiquitin from the USP pocket. We are interested in whether the dynamics of WDR48 influences such processes such that tightening of the ancillary domain around ubiquitin may shift the SLD even closer than its current ~9-Å approach to the USP46 thumb domain and its active-site proximal loops.

The WDR48 SLD has also been implicated in recruitment of USP1 substrate complexes. SUMO-like interacting motifs (SLIM) were identified in FANCI and hELG, respective partners of USP1 substrates FANCD2 and PCNA (Yang et al., 2011). Our structure positions the WDR48 SLD in a plausible orientation relative to the expected position of substrate protein opposite the cradled ubiquitin and WDR48 propeller (Figure 8D). Alignment of a SUMO-interacting motif (SIM) (PDB: 2LAS) onto the WDR48 SLD indicates the expected position of a substrate partner's SLIM peptide (Figure 8C). In the context of such multiprotein complexes, this recruitment and orientation of substrate may contribute to more efficient catalysis in addition to the stimulation provided by the β-propeller interaction.

We provide experimental evidence that the WDR48:USP46 binding mode is conserved across the WDR48-dependent class of USPs. Our structure-based mutations validated the importance of the propeller interface-1, and showed an excellent correlation between diminished binding of WDR48 and impairment of USP deubiquitinase activity. Selected mutations in this WDR48 surface (i.e. K214E/W256A/R272D) that affected USP46 binding and function were also detrimental to USP1. Likewise, mutation of USP1 E444K, analogous to the impactful USP46 E186K mutation, abrogated WDR48 binding and stimulation of USP1 deubiquitinase activity. Homology models of USP1 and USP12 show conserved alignment of several features on the outer tip of the USP fingers domain where WDR48 interaction is observed, while non-WDR48-dependent USPs have poor

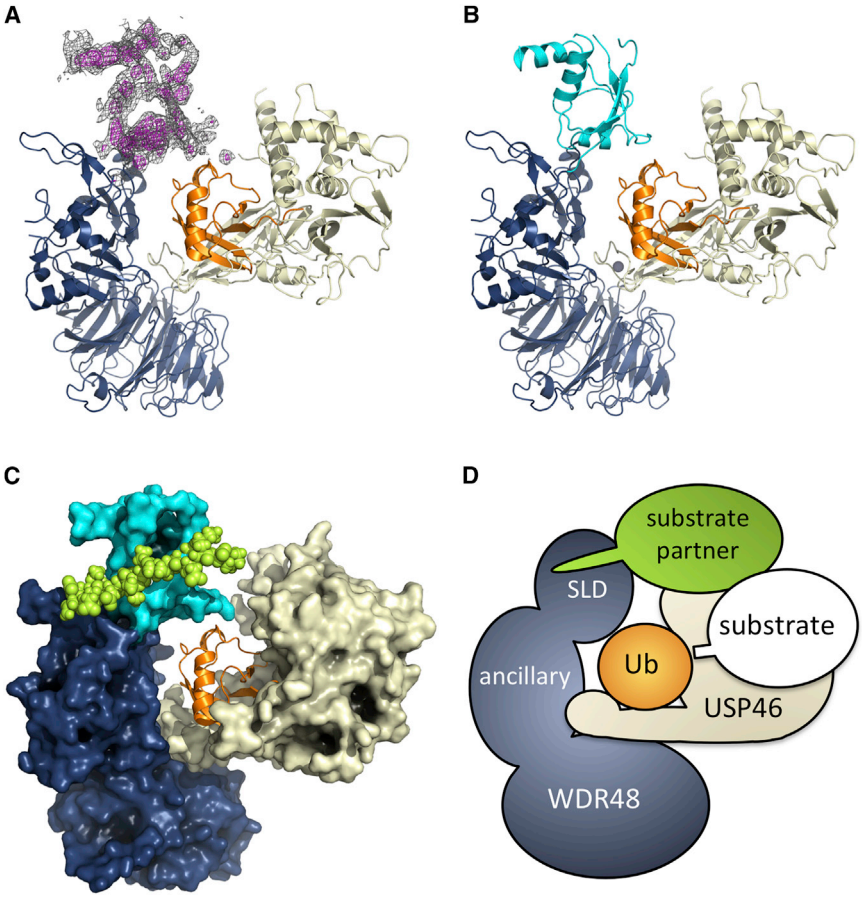

Figure 8. Data and Schematic for a Full-Length WDR48:USP46:Ubiquitin Ternary Complex

(A) 3.9 Å electron density of an F_o-F_c difference map contoured at 3σ (magenta) and 1.5σ (gray) delineates the WDR48 C-terminal domain absent from the search model.

(B) The refined polyalanine build shows a modified SUMO-like domain (SLD) of WDR48 in cyan further encircling the USP46-bound ubiquitin.

(C) Alignment of a SUMO structure (PDB: 2LAS) onto the WDR48 SLD indicates the position of a SUMO-interacting motif (SIM) peptide (bright green, CPK), and thereby the expected location of analogous WDR48 SUMO-like interacting motifs (SLIM) as identified in some USP1 substrate complexes. The molecular surfaces shown for WDR48 and USP46 highlight the relatively enclosed space of the bound ubiquitin (orange).

(D) The schematic suggests relative positions of substrate complexes, wherein an SLIM-bearing partner of the ubiquitinated substrate is recruited by the WDR48 SLD, while the ubiquitinated substrate protein itself is expected to bind in the proximal ubiquitin location on the outer surface of the USP palm/thumb domains.

See also Figure S7.

conservation of this pattern (Figure S8). The unique binding mode elucidated here thus provides a framework to guide further exploration into the role of the larger USP1 insertions and the particular interactions of USP12 and USP46 in mediating their respective biological functions in cancer and signaling. The unexpected position of the WD protein relative to USP and its bound ubiquitin broadens the scope of potential allosteric mechanisms, provides a platform for elucidating therapeutic interventions aimed at the WDR48:USP1 interface, and invigorates our interrogation of the inter-connectedness of components of the USP architecture.

EXPERIMENTAL PROCEDURES

Protein Purification

WT or mutant N-terminal His-tagged WDR48 (1–677, 2–580, or 2–336) and USP46 (25–366) were expressed in baculovirus-infected *Trichoplusia ni* cells, harvested by centrifugation, and stored at −80°C. Cells were lysed in 25 mM Tris (pH 8.0), 150 mM NaCl, 5 mM β-mercaptoethanol (βME), and 5% glycerol. Clarified lysate (40,000 rpm, 1 hr) was loaded on an Ni-nitrilotriacetic acid affinity column (Qiagen) washed with buffer A (50 mM Tris [pH 8.0], 150 mM NaCl) plus 5 mM βME and 10 mM imidazole, and eluted with buffer A plus 300 mM imidazole. Tobacco etch virus-digested protein (buffer A plus 1 mM tris(2-carboxyethyl)phosphine (TCEP), 4°C overnight) was diluted and loaded on a QHP column (GE Healthcare) and eluted by a NaCl gradient in 25 mM Tris (pH 8.0) and 1 mM TCEP. The protein was purified on a HiLoad 16/60 Superdex 200 size-exclusion chromatography (SEC) column (GE Healthcare) equilibrated in buffer B (25 mM Tris [pH 8.0], 100 mM NaCl, 1 mM TCEP). Peak fractions were pooled and concentrated to ~10 mg/ml.

Ubiquitin and ubiquitin 2-bromoethylamine (Ub-BEA) were prepared as described previously (Huang et al., 2012). Reaction of USP46 with Ub-BEA was inefficient without WDR48 present. Therefore, WDR48 was mixed with excess USP46 (25–366) and the complex purified by SEC (HiLoad 16/60 Superdex S200; GE Healthcare) in buffer B. Freshly prepared Ub-BEA was incubated with the concentrated WDR48:USP46 complex for 1–6 hr at room temperature, and again purified by SEC as above to remove excess Ub-BEA. The ternary complex was concentrated to ~20 mg/ml, flash-frozen in liquid nitrogen, and stored at −80°C.

Crystallization

All crystals were grown by hanging-drop vapor diffusion experiments at 19°C using equal ratios of protein and well solutions. All samples were cryoprotected by brief washes in well solution augmented with listed cryoprotectants prior to flash-freezing in liquid nitrogen for data collection.

$WDR48_{2–580}$ crystals were grown by streak-seeding drops set with 0.72 M sodium phosphate, 0.72 M potassium phosphate, 90 mM HEPES (pH 7.5) well solution. Gold derivatives were prepared by soaking individual crystals for 20 min in 0.5 mM Au(I) potassium cyanide (Hampton Research HR2-444-01), 5% glycerol, 0.72 M sodium phosphate, 0.72 M potassium phosphate, and 90 mM HEPES (pH 7.5). Cryoprotectant solution included 20% glycerol.

20 mg/ml $USP46_{25–366}$ with bound Ub-BEA crystallized from a sample including $WDR48_{2–336}$ set against a well solution of 3.6 M sodium formate. Cryoprotectant solution included 25% glycerol.

15 mg/ml $WDR48_{2–580}$:$USP46_{25–366}$:Ub-BEA ternary complex was crystallized in 0.1 M Tris (pH 8.8), 0.1 M NaCl, 5% EtOH, and 15% 2-methyl-2,4-pentanediol (MPD) by streak seeding using crushed initial hit crystals. Cryoprotection was achieved with well solutions augmented to 30% MPD. A similar protocol was successful for crystallization of a full-length $WDR48_{1–677}$:$USP46_{25–366}$:Ub-BEA ternary complex using well solution of 15% MPD, 0.1 M NaCl, 0.1 M HEPES (pH 7.0).

Data Collection and Refinement

Data were collected at Stanford Synchrotron Radiation Lightsource beamline 7-1 (WDR48, 1.02638 Å wavelength) and the Advanced Light Source beamline

5.0.2 (USP46:Ub, 0.9794 Å wavelength; WDR48:USP46:Ub, 1.000 Å wavelength). The novel WDR48 structure was built with phases determined by single-wavelength anomalous diffraction using derivatized gold atoms. Eight gold locations were identified using PHENIX AutoSol (Terwilliger et al., 2009), which allowed construction of the apo protein model that was refined to R/R_{free} of 18.9/23.4 with 0.8% Ramachandran outliers. The ternary complex structure was determined by molecular replacement using the apo WDR48 structure and a USP7:ubiquitin complex (1NBF) as search model, refined to R/R_{free} of 19.5/27.0 with 1.2% Ramachandran outliers. The USP46:ubiquitin structure was determined by molecular replacement using initial search models of the USP46 extracted from the ternary complex and ubiquitin extracted from PDB: 3TMP, and refined to R/R_{free} of 18.9/22.4 with 0.5% Ramachandran outliers. The full-length WDR48:USP46~ubiquitin ternary complex was determined by molecular replacement using the truncated WDR48 ternary complex. Helical features in additional density were used to orient a SUMO structure (PDB: 2LAS) to guide manual construction of a poly-ala trace. At this low resolution, refinement in PHENIX included Ramachandran restraints and use of the higher-resolution structures as reference targets to avoid degradation of geometric terms (R/R_{free} 22.4/27.2, 0.8% Ramachandran outliers). The poly-ala trace is meant to serve as a coarse indicator of the position and topology of the SLD domain, but does not permit detailed atomic analysis. All models were constructed using iterative rounds of manual building in Coot (Emsley and Cowtan, 2004), and refinement in PHENIX (Adams et al., 2010) and Buster (Bricogne et al., 2011) (Table 1).

In Vitro Binding

To assess the binding of WDR48 constructs to USP46, we used biolayer interferometry as implemented in the OctetRed system (ForteBio). Streptavidin tips (ForteBio) were equilibrated in binding buffer (PBS plus 1 mM TCEP or DTT, 0.02% Tween 20, 0.1 mg/ml human serum albumin or BSA), then introduced into 5 μg/ml biotinylated USP46 (200 μl) and loaded to a loading density of approximately 3 nm (well below saturation). Tips were then equilibrated in binding buffer and introduced into wells containing a serial dilution of a WDR48 variant (200 μl). Association was monitored for 5–180 min (depending on the binding kinetics of the variant), then tips were moved to wells containing only binding buffer (200 μl) to monitor dissociation. Zero-analyte controls were performed to correct for drift over the course of each experiment, and these sensorgrams were used to produce background-subtracted curve sets.

Where binding was measurable, it was typically with very slow on- and off-rates such that equilibrium conditions were difficult to achieve. For such non-equilibrium sensorgrams (e.g. WT and L152R/S155W), both the association and dissociation phases were fitted with a 1:1 simple pseudo-first-order interaction model (i.e. $d[\text{Analyte-Ligand}]/dt = k_{on}.[\text{Analyte}].[\text{Ligand}] - k_{off}.[\text{Analyte-Ligand}]$), where [Analyte-Ligand] is complex formed. Variables k_{on} and k_{off} were constrained to globally fit values over the curve set. The R_{max} was allowed local values for each curve, as the density of immobilized ligand varies slightly with each curve owing to the use of separate measuring probes for each measured curve. For the S170Y mutant, the dissociation phase was too rapid to accurately measure; however, this weaker binding mutant did achieve equilibrium conditions. As such, we applied a steady-state model ($R_{eq} = (R_{max}.[\text{Analyte}])/([\text{Analyte}] + K_D)$, where R_{eq} is the response at equilibrium, R_{max} is the response at saturation, and [Analyte] is the concentration of analyte, which is fixed with respect to time) to the steady-state region (time >200 s) of the curves. Both R_{max} and K_D were constrained to single global values. Kinetic constants for S170Y were also determined by fitting the association phases to a first-order integrated rate equation to determine k_{obs} at various S170Y concentrations. We then used the linear relationship between k_{obs} and S170Y concentration to determine k_{on} and k_{off}, and thus K_D. A similar kinetic analysis was employed to quantify the weak interaction between USP46 E186K and $WDR48_{3X}$.

In Vitro Deubiquitination Activity

To assess the deubiquitinating activity of the USP46:WDR48 complex, we used a ubiquitin-AMC cleavage assay. Complexes of USP46 and WDR48 were formed by incubating the proteins at 400 nM USP46 and either 400 nM or 8,000 nM WDR48 overnight at 4°C. Complexes were then mixed 1:1 with serial dilutions of Ub-AMC (Boston Biochem). The total reaction volume was 14 μl per well in a 384-well plate (ProxiPlate-384 F Plus; PerkinElmer), and assays were carried out in PBS with 1 mM TCEP, 0.02% Tween 20, and 0.1 mg/ml human serum albumin. We monitored the release of AMC using an excitation wavelength of 345 nm and monitoring emission at 445 nm with a 435-nm cutoff filter. Readings were taken for 1 hr using a SpectraMax M5e plate reader (Molecular Devices). We determined the slope of the linear regions (from 2,000 to 3,600 s) using linear regression in Kaleidagraph, and converted fluorescence signal to μmol AMC using an AMC standard curve. Rates (in μmol/s) were plotted as a function of Ub-AMC concentration. Due to the weak activity of USP46 we were not able to achieve saturation, and therefore unable to report rigorous values for K_M and k_{cat}. Data were fit to a line to determine k_{cat}/K_M.

Cellular Deubiquitination Assays

293T cells were transfected for 48 hr with HA-ubiquitin, FLAG-ID2, and untagged USP1 (WT, E444K, or C90S) using FuGENE HD (Promega). Cells were treated with 10 μM MG-132 for 60 min prior to lysis in NP40 lysis buffer (1% NP-40, 120 mM NaCl, 50 mM Tris-HCl [pH 7.5], 1 mM EDTA) containing 10 μM MG-132, 10 mM *N*-ethylmaleimide, protease inhibitor cocktail (Roche), and phosphatase inhibitor cocktail (Roche). Soluble lysates were denatured with 1% SDS at 95°C for 5 min and then diluted 20-fold in lysis buffer. FLAG-ID2 was immunoprecipitated using anti-M2 FLAG agarose (Sigma-Aldrich) for 4 hr. Beads were washed in lysis buffer and bound proteins eluted with LDS sample buffer.

Co-immunoprecipitation

293T cells were transfected with FLAG-USP1 and HA-WDR48 using FuGENE HD (Promega) for 48 hr and lysed in Triton lysis buffer (1% Triton, 20 mM Tris-HCl [pH 7.5], 135 mM NaCl, 1.5 mM $MgCl_2$, 1 mM EGTA, 10% glycerol) containing protease inhibitor cocktail (Roche) and phosphatase inhibitor cocktail (Roche). Soluble lysate was incubated with anti-M2 FLAG agarose (Sigma-Aldrich) for 4 hr. Beads were washed in lysis buffer and bound proteins eluted with LDS sample buffer.

Antibodies

Anti-FLAG (Sigma), anti-USP1 (clone 5 × 10^{10}; in-house GNE antibody), anti-HA (Cell Signaling), anti-WDR48 (clone 9F10; in-house GNE antibody), actin (clone C4; MP Biomedicals).

ACCESSION NUMBERS

Coordinates and structure factors are deposited at the PDB under accession codes PDB: 5CVL, 5CVM, 5CVN, and 5CVO for $WDR48_{2–580}$, $USP46_{25–366}$~ubiquitin, $WDR48_{2–580}$:$USP46_{25–366}$~ubiquitin, and WDR48:$USP46_{25–366}$~ubiquitin, respectively.

SUPPLEMENTAL INFORMATION

Supplemental Information includes eight figures and can be found with this article online at http://dx.doi.org/10.1016/j.str.2015.08.010.

AUTHOR CONTRIBUTIONS

J.Y. purified and crystallized proteins. S.F.H. determined the structures. A.S. and E.D. performed in vitro binding and kinetics. K.W. and K.N. performed cellular USP1 assays. M.A.S. aided project conception. S.F.H. wrote the paper with help from the other authors.

ACKNOWLEDGMENTS

We thank X. Ma and B. Maurer for characterizations of USP1, the Genentech Structural Biology Expression Group for cloning and expression of constructs, and J. Kiefer and V. Dixit for comments. Portions of this research were carried out at the Advanced Light Source (ALS) and the Stanford Synchrotron Radiation Lightsource (SSRL). The ALS is supported by the Director, Office of Science, Office of Basic Energy Sciences, of the U.S. Department of Energy under Contract No. DE-AC02-05CH11231. The SSRL is supported by the DOE Office of Biological and Environmental Research, and by the NIH, National Institute of General Medical Sciences (including P41GM103393), and the National Center

for Research Resources (P41RR0001209). All authors are employees of Genentech, Inc.

Received: March 25, 2015
Revised: July 27, 2015
Accepted: August 4, 2015
Published: September 17, 2015

REFERENCES

Adams, P.D., Afonine, P.V., Bunkóczi, G., Chen, V.B., Davis, I.W., Echols, N., Headd, J.J., Hung, L.-W., Kapral, G.J., Grosse-Kunstleve, R.W., et al. (2010). PHENIX: a comprehensive Python-based system for macromolecular structure solution. Acta Crystallogr. D Biol. Crystallogr. *66*, 213–221.

Avvakumov, G.V., Walker, J.R., Xue, S., Finerty, P.J., Mackenzie, F., Newman, E.M., and Dhe-Paganon, S. (2006). Amino-terminal dimerization, NRDP1-rhodanese interaction, and inhibited catalytic domain conformation of the ubiquitin-specific protease 8 (USP8). J. Biol. Chem. *281*, 38061–38070.

Bingol, B., Tea, J.S., Phu, L., Reichelt, M., Bakalarski, C.E., Song, Q., Foreman, O., Kirkpatrick, D.S., and Sheng, M. (2014). The mitochondrial deubiquitinase USP30 opposes parkin-mediated mitophagy. Nature *510*, 370–375.

Bricogne, G., Blanc, E., Brandl, M., Flensburg, C., Keller, P., Paciorek, W., Roversi, P., Sharff, A., Smart, O.S., Vonrhein, C., et al. (2011). BUSTER Version 2.11.4 (Global Phasing Ltd).

Chen, J., Dexheimer, T.S., Ai, Y., Liang, Q., Villamil, M.A., Inglese, J., Maloney, D.J., Jadhav, A., Simeonov, A., and Zhuang, Z. (2011). Selective and cell-active inhibitors of the USP1/UAF1 deubiquitinase complex reverse cisplatin resistance in non-small cell lung cancer cells. Chem. Biol. *18*, 1390–1400.

Cohn, M.A., Kowal, P., Yang, K., Haas, W., Huang, T.T., Gygi, S.P., and D'Andrea, A.D. (2007). A UAF1-containing multisubunit protein complex regulates the Fanconi anemia pathway. Mol. Cell *28*, 786–797.

Cohn, M.A., Kee, Y., Haas, W., Gygi, S.P., and D'Andrea, A.D. (2009). UAF1 is a subunit of multiple deubiquitinating enzyme complexes. J. Biol. Chem. *284*, 5343–5351.

Emsley, P., and Cowtan, K. (2004). Coot: model-building tools for molecular graphics. Acta Crystallogr. D Biol. Crystallogr. *60*, 2126–2132.

Faesen, A.C., Dirac, A.M.G., Shanmugham, A., Ovaa, H., Perrakis, A., and Sixma, T.K. (2011a). Mechanism of USP7/HAUSP activation by its C-terminal ubiquitin-like domain and allosteric regulation by GMP-synthetase. Mol. Cell *44*, 147–159.

Faesen, A.C., Luna-Vargas, M.P.A., Geurink, P.P., Clerici, M., Merkx, R., van Dijk, W.J., Hameed, D.S., El Oualid, F., Ovaa, H., and Sixma, T.K. (2011b). The differential modulation of USP activity by internal regulatory domains, interactors and eight ubiquitin chain types. Chem. Biol. *18*, 1550–1561.

Gangula, N.R., and Maddika, S. (2013). WD repeat protein WDR48 in complex with deubiquitinase USP12 suppresses Akt-dependent cell survival signaling by stabilizing PH domain leucine-rich repeat protein phosphatase 1 (PHLPP1). J. Biol. Chem. *288*, 34545–34554.

García-Santisteban, I., Zorroza, K., and Rodríguez, J.A. (2012). Two nuclear localization signals in USP1 mediate nuclear import of the USP1/UAF1 complex. PLoS One *7*, e38570.

García-Santisteban, I., Peters, G.J., Giovannetti, E., and Rodríguez, J.A. (2013). USP1 deubiquitinase: cellular functions, regulatory mechanisms and emerging potential as target in cancer therapy. Mol. Cancer *12*, 91.

Hershko, A., Eytan, E., Ciechanover, A., and Haas, A.L. (1982). Immunochemical analysis of the turnover of ubiquitin-protein conjugates in intact cells. Relationship to the breakdown of abnormal proteins. J. Biol. Chem. *257*, 13964–13970.

Holm, L., and Sander, C. (1995). Dali: a network tool for protein structure comparison. Trends Biochem. Sci. *20*, 478–480.

Hu, M., Li, P., Li, M., Li, W., Yao, T., Wu, J.-W., Gu, W., Cohen, R.E., and Shi, Y. (2002). Crystal structure of a UBP-family deubiquitinating enzyme in isolation and in complex with ubiquitin aldehyde. Cell *111*, 1041–1054.

Hu, M., Li, P., Song, L., Jeffrey, P.D., Chenova, T.A., Wilkinson, K.D., Cohen, R.E., and Shi, Y. (2005). Structure and mechanisms of the proteasome-associated deubiquitinating enzyme USP14. EMBO J. *24*, 3747–3756.

Huang, T.T., Nijman, S.M.B., Mirchandani, K.D., Galardy, P.J., Cohn, M.A., Haas, W., Gygi, S.P., Ploegh, H.L., Bernards, R., and D'Andrea, A.D. (2006). Regulation of monoubiquitinated PCNA by DUB autocleavage. Nat. Cell Biol. *8*, 339–347.

Huang, O.W., Ma, X., Yin, J., Flinders, J., Maurer, T., Kayagaki, N., Phung, Q., Bosanac, I., Arnott, D., Dixit, V.M., et al. (2012). Phosphorylation-dependent activity of the deubiquitinase DUBA. Nat. Struct. Mol. Biol. *19*, 171–175.

Joo, H.-Y., Jones, A., Yang, C., Zhai, L., Smith, A.D., Zhang, Z., Chandrasekharan, M.B., Sun, Z.-W., Renfrow, M.B., Wang, Y., et al. (2011). Regulation of histone H2A and H2B deubiquitination and Xenopus development by USP12 and USP46. J. Biol. Chem. *286*, 7190–7201.

Kee, Y., Yang, K., Cohn, M.A., Haas, W., Gygi, S.P., and D'Andrea, A.D. (2010). WDR20 regulates activity of the USP12 x UAF1 deubiquitinating enzyme complex. J. Biol. Chem. *285*, 11252–11257.

Köhler, A., Zimmerman, E., Schneider, M., Hurt, E., and Zheng, N. (2010). Structural basis for assembly and activation of the heterotetrameric SAGA histone H2B deubiquitinase module. Cell *141*, 606–617.

Komander, D., and Rape, M. (2012). The ubiquitin code. Annu. Rev. Biochem. *81*, 203–229.

Komander, D., Clague, M.J., and Urbé, S. (2009). Breaking the chains: structure and function of the deubiquitinases. Nat. Rev. Mol. Cell Biol. *10*, 550–563.

Lehoux, M., Gagnon, D., and Archambault, J. (2014). E1-mediated recruitment of a UAF1-USP deubiquitinase complex facilitates human papillomavirus DNA replication. J. Virol. *88*, 8545–8555.

Liang, Q., Dexheimer, T.S., Zhang, P., Rosenthal, A.S., Villamil, M.A., You, C., Zhang, Q., Chen, J., Ott, C.A., Sun, H., et al. (2014). A selective USP1-UAF1 inhibitor links deubiquitination to DNA damage responses. Nat. Chem. Biol. *10*, 298–304.

McClurg, U.L., Summerscales, E.E., Harle, V.J., Gaughan, L., and Robson, C.N. (2014). Deubiquitinating enzyme Usp12 regulates the interaction between the androgen receptor and the Akt pathway. Oncotarget *5*, 7081–7092.

Molland, K., Zhou, Q., and Mesecar, A.D. (2014). A 2.2 Å resolution structure of the USP7 catalytic domain in a new space group elaborates upon structural rearrangements resulting from ubiquitin binding. Acta Crystallogr. F Struct. Biol. Commun. *70*, 283–287.

Murai, J., Yang, K., Dejsuphong, D., Hirota, K., Takeda, S., and D'Andrea, A.D. (2011). The USP1/UAF1 complex promotes double-strand break repair through homologous recombination. Mol. Cell. Biol. *31*, 2462–2469.

Nijman, S.M.B., Huang, T.T., Dirac, A.M.G., Brummelkamp, T.R., Kerkhoven, R.M., D'Andrea, A.D., and Bernards, R. (2005). The deubiquitinating enzyme USP1 regulates the Fanconi anemia pathway. Mol. Cell *17*, 331–339.

Olazabal-Herrero, A., García-Santisteban, I., and Rodríguez, J. (2015). Structure-function analysis of USP1: insights into the role of Ser313 phosphorylation site and the effect of cancer-associated mutations on autocleavage. Mol. Cancer *14*, 33.

Park, E., Kim, J.M., Primack, B., Weinstock, D.M., Moreau, L.A., Parmar, K., and D'Andrea, A.D. (2013). Inactivation of Uaf1 causes defective homologous recombination and early embryonic lethality in mice. Mol. Cell. Biol. *33*, 4360–4370.

Reyes-Turcu, F.E., and Wilkinson, K.D. (2009). Polyubiquitin binding and disassembly by deubiquitinating enzymes. Chem. Rev. *109*, 1495–1508.

Samara, N.L., Datta, A.B., Berndsen, C.E., Zhang, X., Yao, T., Cohen, R.E., and Wolberger, C. (2010). Structural insights into the assembly and function of the SAGA deubiquitinating module. Science *328*, 1025–1029.

Sowa, M.E., Bennett, E.J., Gygi, S.P., and Harper, J.W. (2009). Defining the human deubiquitinating enzyme interaction landscape. Cell *138*, 389–403.

Teixeira, L.K., and Reed, S.I. (2013). Ubiquitin ligases and cell cycle control. Annu. Rev. Biochem. *82*, 387–414.

Terwilliger, T.C., Adams, P.D., Read, R.J., McCoy, A.J., Moriarty, N.W., Grosse-Kunstleve, R.W., Afonine, P.V., Zwart, P.H., and Hung, L.-W. (2009). Decision-making in structure solution using Bayesian estimates of map

quality: the PHENIX AutoSol wizard. Acta Crystallogr. D Biol. Crystallogr. *65*, 582–601.

Villamil, M.A., Chen, J., Liang, Q., and Zhuang, Z. (2012a). A noncanonical cysteine protease USP1 is activated through active site modulation by USP1-associated factor 1. Biochemistry *51*, 2829–2839.

Villamil, M.A., Liang, Q., Chen, J., Choi, Y.S., Hou, S., Lee, K.H., and Zhuang, Z. (2012b). Serine phosphorylation is critical for the activation of ubiquitin-specific protease 1 and its interaction with WD40-repeat protein UAF1. Biochemistry *51*, 9112–9123.

Villamil, M.A., Liang, Q., and Zhuang, Z. (2013). The WD40-repeat protein-containing deubiquitinase complex: catalysis, regulation, and potential for therapeutic intervention. Cell Biochem. Biophys. *67*, 111–126.

Williams, S.A., Maecker, H.L., French, D.M., Liu, J., Gregg, A., Silverstein, L.B., Cao, T.C., Carano, R.A.D., and Dixit, V.M. (2011). USP1 deubiquitinates ID proteins to preserve a mesenchymal stem cell program in osteosarcoma. Cell *146*, 918–930.

Xu, C., and Min, J. (2011). Structure and function of WD40 domain proteins. Protein Cell *2*, 202–214.

Yang, K., Moldovan, G.-L., Vinciguerra, P., Murai, J., Takeda, S., and D'Andrea, A.D. (2011). Regulation of the Fanconi anemia pathway by a SUMO-like delivery network. Genes Dev. *25*, 1847–1858.

Ye, Y., Scheel, H., Hofmann, K., and Komander, D. (2009). Dissection of USP catalytic domains reveals five common insertion points. Mol. Biosyst. *5*, 1797–1808.

 ©2015 Elsevier Ltd All rights reserved